PROTECTIVE ROLE OF L-CARNITINE AGAINST METHOTREXATE-INDUCED SIDE EFFECTS ON SUBMANDIBULAR GLAND IN ADULT MALE ALBINO RATS

Mary Refaat Isaac[1], Gamal T. Abdelhady[1] and Enas Haridy Ahmed[1&2]

[1]Department of Anatomy and Embryology, Faculty of Medicine, Ain Shams University, Cairo, Egypt
[2]Department of Anatomy, Faculty of Medicine, University of Hail, Hail, KSA

Corresponding author:
Mary Refaat Isaac
Mobile: +2 01001171964
E-mail:
drmaryrefaat@yahoo.com

Received: 30/03/2024
Accepted: 28/04/2024

Online ISSN: 2735-3540

ABSTRACT:

Background: *Submandibular gland impairment is a common side effect of methotrexate (MTX). L-carnitine (LC) is an antioxidant that is widely used nowadays as a protective against chemotherapeutic drugs' hazards.*

Aim of the work: *examine the potential protective effect of LC on MTX induced submandibular gland injury.*

Material and methods: *Thirty-six adult male albino rats, aging 4-6 months and weighing 200-250 gm, were used. Animals were divided into three groups.* ***Group I:*** *control group and was further subdivided into four subgroups 6 rats each.* ***Group II:*** *included 6 rats which received 20mg/kg MTX intraperitoneally on the first day.* ***Group III:*** *included 6 rats which received 20mg/kg MTX intraperitoneally on the first day and oral 100 mg/kg LC once daily from first till fifth day. After 5 days, animals were anesthetized, and submandibular glands were excised and processed for histological, ultrastructural, immunohistochemical and morphometric studies.*

Results: *Methotrexate induced marked distortion and separation of the gland's histoarchitecture with congestion, connective tissue fibers' aggregation and cellular infiltration. Ultra-structurally, acinar and striated ductal cells revealed degenerative nuclear changes, marked cytoplasmic vacuolation and indistinct organelles. Morphometric analysis revealed highly significant decrease in Ki-67 immune stain. However, rats given LC with MTX had marked preservation of glandular histoarchitecture and significant increase in Ki-67 immune expression.*

Conclusion: *L-carnitine exerted a marked protective role against MTX induced submandibular histoarchitectural changes. Thus, it could be considered as a highly promising protective agent against MTX-induced xerostomia in cancer and RA arthritis patients.*

Keywords*: Submandibular gland, methotrexate, L-Carnitine, xerostomia*

INTRODUCTION:

Chemotherapeutic drugs have nonselective cytotoxic effects thus can harm healthy as well as cancerous cells. The degree of harm varies according to treatment modality, dose, and duration [(1)]. Methotrexate (MTX), a folic acid antagonist, is considered as a golden cytotoxic drug in the management of malignancies and some autoimmune disorders, among which is rheumatoid arthritis (RA) [(2)].

However, despite being inexpensive and highly effective as an antiproliferative and anti-inflammatory drug, its clinical utilization could be limited due to its associated side effects which could affect the patients' quality of life [3]. Submandibular gland hypofunction with subsequent xerostomia has been reported as one of the most disturbing side effects of MTX [4]. Xerostomia leads to disturbance of swallowing, taste, and speech as well as oral and dental hygiene leading to periodontitis, gingivitis, leucoplakia, and even cancer. These effects usually have psychological impacts and limitation in the quality of life of the affected individuals [5].

In addition, some of the autoimmune diseases treated by MTX are already associated with xerostomia. Among these diseases is RA where dry mouth is considered as one of its commonly encountered symptoms [6].

The cytotoxic mechanism of MTX is based on disturbing the antioxidant defence system and thus increasing the vulnerability of cells to reactive oxygen species (ROS) [7]. It has been postulated that oxidative stress was involved in submandibular gland dysfunction and subsequent alterations including xerostomia [4]. Therefore, different antioxidants might prevent MTX induced cell damage [7].

L-Carnitine (LC) is a potent protective antioxidant [8]. It is synthesised endogenously, from the essential amino acids, methionine, and lysine, by some organs including brain, liver, and kidneys [9]. It has been widely used nowadays either as a pharmacological or a nutritional supplement that has been found markedly advantageous in various conditions [10] including uremia [11] treatment of obesity [12], decreasing intolerance of glucose [13]. And in treatment of multiple neurological diseases, including Alzheimer's disease, Parkinson disease, hepatic encephalopathy, autism spectrum disorder, and other painful neuropathies [14].

It has been also reported that it had a protective role against many chemotherapeutic drugs thus ameliorating their hazardous side effects [15]. Among these is its ability to prevent MTX induced leukocyte death [7] and various organ injuries including gastrointestinal complications that occur during treatment of RA arthritis patients [16].

AIM OF THE WORK

In view of the above findings, the present study was designed to examine the potential protective effect of LC on MTX induced submandibular gland injury.

MATERIAL AND METHODS

Drugs:

1. Methotrexate: Methotrexate MYLAN 50mg/2ml ampoules, obtained from Mylan Pharmaceutical Industry Company, USA. It was given in a dose equivalent to 20mg/kg by intraperitoneal injection [7]. Thus, each rat was given 0.16-0.2ml of each ampoule according to its weight.

2. L-Carnitine: Carnitol 500 mg capsules, purchased from Global Napi Company for pharmaceutical and chemical industries. Each capsule was dissolved in 50ml distilled water to get a solution of 10mg/ml concentration. Each rat was given 2-2.5 of the prepared solution which is equivalent to a dose of 100 mg/kg body weight [17] by gastric gavage.

Animals:

Thirty-six male Wistar strain albino rats aging 4 - 6 months and weighing 200-250 grams were obtained and bred in the Animal House of Faculty of Medicine Ain Shams Research Institute (MASRI). Rats were housed in conventional 30 x 35 cm wire-mesh cages, 2 rats/cage. They were kept at room temperature with regular light/dark cycles with good ventilation and suitable

environmental conditions and had free access to water and daily diet. Animals were allowed to acclimatize to experimental conditions by housing them for 10 days prior to experiment.

Experimental Protocol:

Animals were divided randomly into three groups as follows:

➢ ***Group I (Control group)*:** consisted of 24 rats and was further equally subdivided into 4 subgroups 6 rats in each:

- **Subgroup IA:** rats were left without any interventions.
- **Subgroup IB:** rats received 0.16-0.2 ml of physiological saline (0.9% NaCl) by intraperitoneal injection on day one of the experiment to simulate the stress of injection.
- **Subgroup IC:** rats received 2-2.5 ml of distilled water, which was the vehicle used for LC, once daily for 5 days by intragastric gavage needle.
- **Subgroup ID:** rats received 100 mg/kg body weight LC, dissolved in distilled water, once daily for 5 days by intragastric gavage needle.

➢ ***Group II (MTX treated group)***: consisted of 6 rats that received intraperitoneal injection of MTX in a dose of 20mg/kg on day one of the experiment.

➢ ***Group III (LC and MTX treated group)***: consisted of 6 rats that received intraperitoneal injection of MTX on day one and LC by intragastric gavage needle once daily from the first till the fifth day of the experiment.

Retrieval of the submandibular glands:

At the end of the experiment, all rats were anaesthetized using intraperitoneal injection of 7mg/kg body weight thiopental sodium then sacrificed by cervical dislocation. Midline incision was done in the neck and submandibular glands were dissected out and cut longitudinally into two equal halves. One half was processed for histological and immunohistochemical studies and the other one for ultrastructural studies.

Histological and immunohistochemical techniques:

Specimens for light microscopic studies were fixed in 10% formalin for one week followed by dehydration in ascending grades of ethanol, then cleared in xylol, impregnated, and embedded in paraffin blocks. Sections of 5 µm in thickness were cut and stained with Hematoxylin and Eosin Stain [(18)].

Other sections from the paraffin blocks were cut and deparaffinized using 0.01% H2O2 then were incubated in a 0.01 M citrate buffer at PH 6 for 10 minutes followed by ethanol for 10 minutes. After that, sections were incubated overnight at 4°C with Ki-67 monoclonal mouse antibodies (using diluted primary antibodies at dilutions of 1/500 and 1/100). Incubation with the avidin biotin complex reagent was then done for one hour followed a peroxidase solution for 6–10 minutes. Finally, a counter stain of Mayer's hematoxylin was utilized [(19)].

Tissue sections were then examined by Olympus light microscope of Histology department, faculty of Medicine, Ain Shams University and positive immune reactivity results were marked by brown coloration of the nuclei.

Ultrathin Techniques:

Specimens for electron microscopic studies, were immediately cut into cubes (1mm in diameter) and fixed overnight in 2.5% phosphate-buffered glutaraldehyde (pH 7.3) at 4°C. They were then postfixed in 1% buffered osmium tetroxide for two hours followed by dehydration in ascending grades of ethyl alcohol and were finally embedded in Epon. Semithin sections 1 µm in thickness were cut with a glass knife and stained with toluidine blue [(20)] and then examined by the same Olympus light microscope to choose the desired areas.

Ultrathin sections 50 nm of the selected areas were cut using a glass knife, mounted on copper grids, stained with uranyl acetate for 20 minutes and lead citrate for 10 minutes, and then they were washed in distilled water & preserved in labeled capsules [20]. The sections were then examined and photographed by transmission electron microscope in the Faculty of Science, Ain Shams University.

Morphometric and statistical analysis:

Examination of six different fields, at x100 magnification, from six different stained slides of six different rats in each group was done to measure the mean area percentage of Ki-67 immunoreactivity using Image J software on RGB stacks of the photomicrographs. Adjustment of threshold was done in overlapping a binary mask on the immune positive areas.

Analysis of morphometric data was done using the statistical package for the social sciences (SPSS) program-version 17-USA, where mean, standard deviation (SD), analyses of variance (ANOVA test), and T-test were done. The $P < 0.001$ indicated high significance, <0.05 indicated significance and >0.05 was considered insignificant.

To exclude bias, images were studied by a neutral examiner who did not know the coding of the study groups.

Ethical Consideration:

Experimental design and protocols were conducted following the guidelines of the Committee of Animal Research Ethics - Faculty of Medicine - Ain Shams University. Ethical committee approval number: FMASU R50/2023.

RESULTS:

➢ Histological Results:

☆ *Group I (Control Group):*

Examination of sections of the four control subgroups revealed almost similar structure of the submandibular gland.

Light microscopic examination of H&E-stained sections showed that the gland was made up of many lobules separated by thin fibrous septa. These lobules had secretory portion made up of almost predominantly serous acini Figure (1) with well-defined outline and lined by pyramidal cells, with basophilic cytoplasm and rounded basal nuclei Figure (2). Regarding the duct system, variable sized acidophilic ducts were seen including intercalated ducts with rounded lumina lined by low cuboidal epithelium and central rounded nuclei Figure (1), striated ducts with almost rounded lumina lined by columnar epithelium with characteristic basal striations with central rounded vesicular nuclei Figures (1&2) and large excretory ducts with wide lumina lined by pseudostratified columnar epithelium Figure (1).

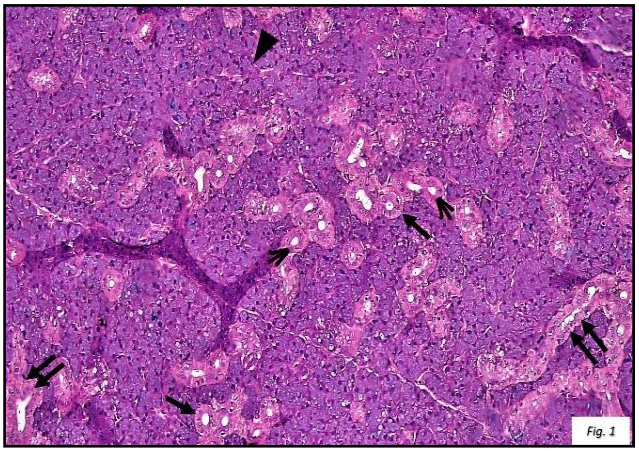

Figure 1: A photomicrograph of a section of rat's submandibular gland of group I (control group) showing acidophilic ducts distributed among basophilic serous acini (Δ). Notice intercalated ducts (⋀) with low cuboidal epithelium and central rounded nuclei, striated ducts (↑) with columnar epithelium, basal striations and central rounded nuclei and the large excretory ducts (↑↑) with pseudostratified columnar epithelium and wide lumina. (H&E X100)

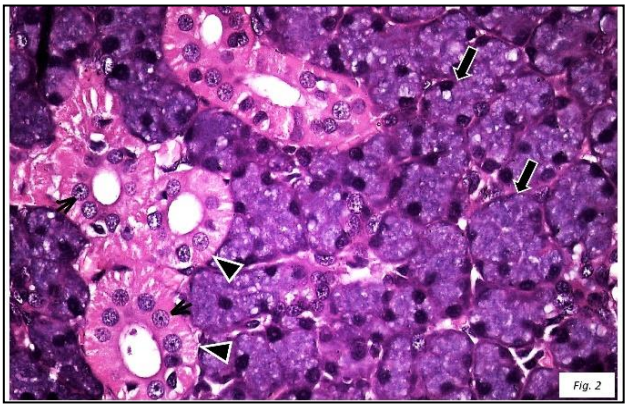

Figure 2: A photomicrograph of a section of rat's submandibular gland of group I (control group) showing well defined acini lined by pyramidal cells, with basophilic cytoplasm and rounded basal nuclei (↑). Notice the striated ducts lined by columnar acidophilic cells with rounded central vesicular nuclei (⩚) and characteristic basal striations (Δ). (H&E X400)

Immune stained sections for Ki-67 protein showed strong positive reaction which was more evident in the glandular ductal system. Scattered nuclear reactivities were also seen in few secretory acini Figure (3).

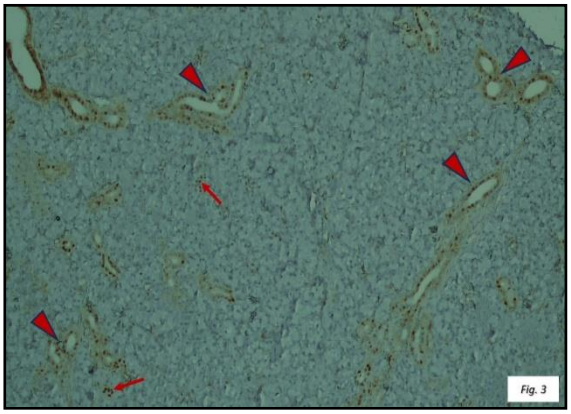

Figure 3: A photomicrograph of a section of rat's submandibular gland of group I (control group) showing strong positive reaction to Ki-67 protein in the ducts and some secretory acini. (Anti Ki-67 antibodies immunostaining X100)

Semithin sections showed serous acini with central lumen surrounded by pyramidal cells with pale cytoplasm and basal rounded to oval nuclei. Striated ducts appeared lined by columnar cells with basal striations and central rounded vesicular nuclei Figure (4).

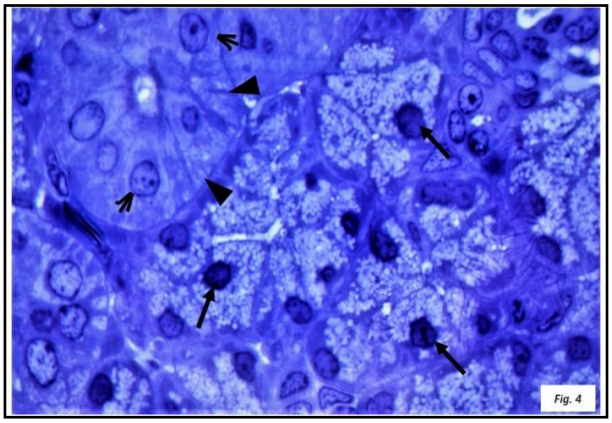

Figure 4: A photomicrograph of a section of rat's submandibular gland of group I (control group) showing serous acini lined by pyramidal cells with pale stained cytoplasm and basal nuclei (↑). Notice the striated ducts lined by columnar cells with basal striations (Δ) and central rounded vesicular nuclei (⩚). (Toluidine blue X1000)

Ultrastructural examination further clarified the structure of acini and striated ducts. Serous acini had rounded to oval euchromatic nuclei, with prominent nucleoli surrounded by arrays of rough endoplasmic reticulum (rER) Figure (5) and rounded to oval mitochondria Figure (6). Numerus large almost rounded electron dense secretory granules were also observed at the apical parts of acinar cells Figures (5&6) close to their luminal surface which showed finger like projecting microvilli Figure (6). The acini were lined by thin regular basal lamina and myoepithelial cells with oval flattened nuclei were seen at the acinar basal side Figure (5).

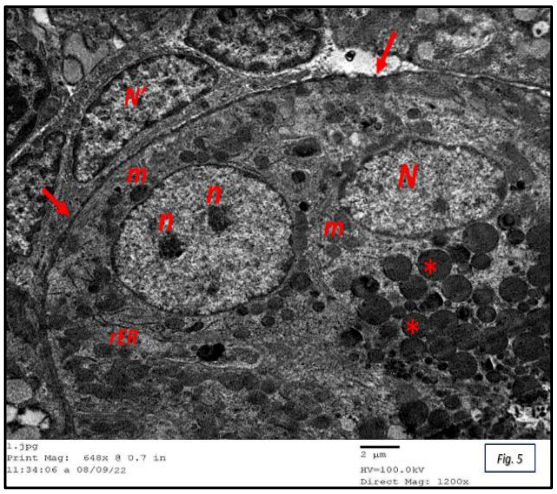

Figure 5: An electronmicrograph of a section of rat's submandibular gland of group I (control group) showing serous acinar cells with euchromatic nuclei (N) and one containing prominent nucleoli (n). Notice the mitochondria (m), the apical large, rounded electron dense secretory granules (*). Notice the thin regular basal lamina (↑) and the myoepithelial cell located at the basal side of the acinus and having an oval flattened nucleus (N'). (Uranyl acetate & lead citrate x1200)

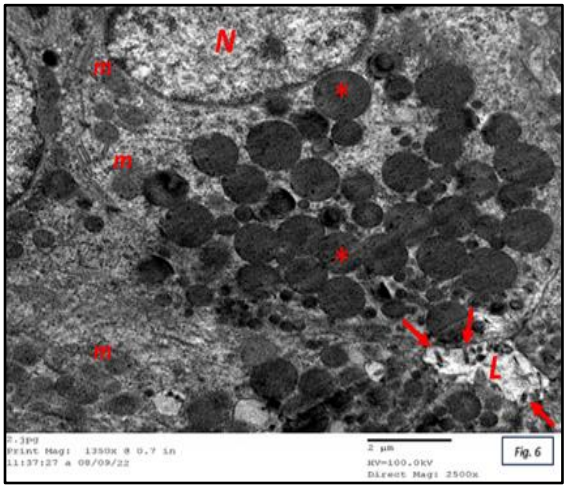

Figure 6: An electronmicrograph of section of rat's submandibular gland of group I (control group) showing serous acinar cell with euchromatic nuclei (N), rounded to oval mitochondria (m), large, rounded electron dense secretory granules (*) and the apical finger like microvilli (↑) projecting towards the lumen (L). (Uranyl acetate & lead citrate x2500)

Striated ducts were lined by tall columnar cells with rounded central euchromatic nuclei Figure (7) with surrounding arrays of rER and mitochondria Figure (7). These ductal cells are characterized by extensive interdigitating basal membrane infoldings with arrays of assorted mitochondria aligned and incorporated within these basal striations. They were either rounded or oval with prominent cristae Figure (8). Apical small and numerous vesicles with variable electron densities were also observed close to the lumen Figure (7).

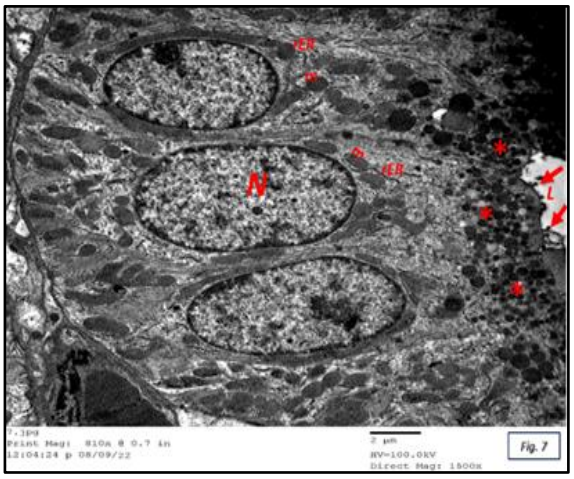

Figure 7: An electronmicrograph of a section of rat's submandibular gland of group I (control group) showing striated duct with lumen (L) surrounded by tall columnar cells with rounded to oval (N) central euchromatic nuclei (N) with adjacent mitochondria (m) and rER (rER). Notice the apical side of ductal cell studded with numerous secretory granules (*) with different sizes and variable electron densities with nearby finger like projecting microvilli (↑). (Uranyl acetate & lead citrate x1500)

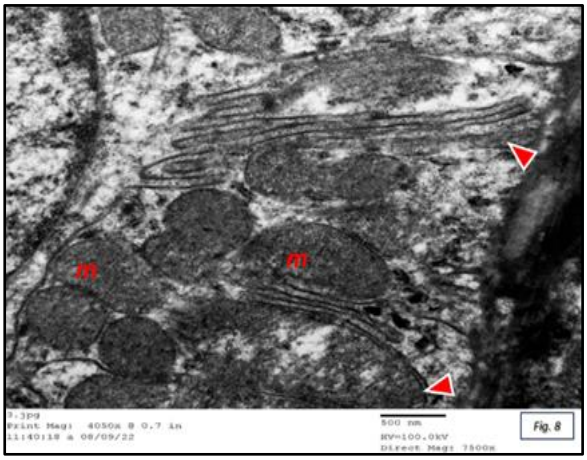

Figure 8: Electronmicrographs of sections of rat's submandibular gland of group I (control group) showing basal part of striated ductal cell with numerous rounded to oval mitochondria (m) with regular cristae incorporated within basal infoldings (Δ). (TEM x7500)

☆ ***Group II (MTX Group):***

Light microscopic examination of H&E-stained sections revealed marked disturbance of the glandular architecture with areas of separation in the glandular tissue Figure (9). Acinar system showed evident disarrangement Figure (9) and indistinct outline of most of the acini Figure (10). Ductal system showed loss of regular cellular arrangement, ill-defined nuclei with areas of focal detachment of epithelial lining Figure (10). Numerous clusters of closely packed disorganized cells Figures (9&10) together with aggregations of connective tissue fibers studded with cellular infiltration Figure (9) were also observed. Moreover, the presence of dilated congested blood vessels was almost a frequent finding Figure (9).

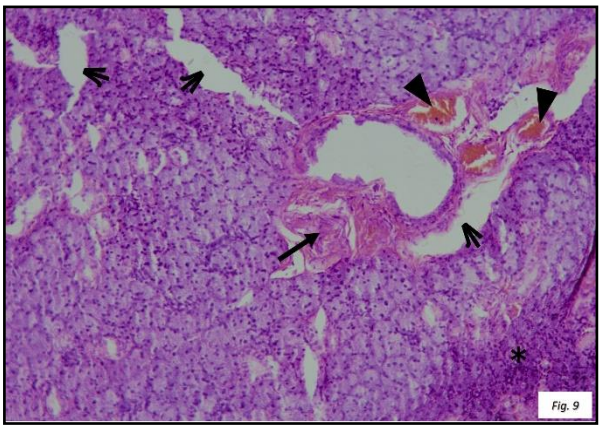

Figure 9: A photomicrograph of a section of rat's submandibular gland of group II (MTX group) showing disturbance of glandular architecture with acinar disarrangement and intervening groups of closely packed disorganized cells (*) . Notice the areas of glandular tissue separation (⋔), the dilated congested blood vessels (Δ) and the aggregations of connective tissue fibers studded with cellular infiltration (↑). (H&E x 100)

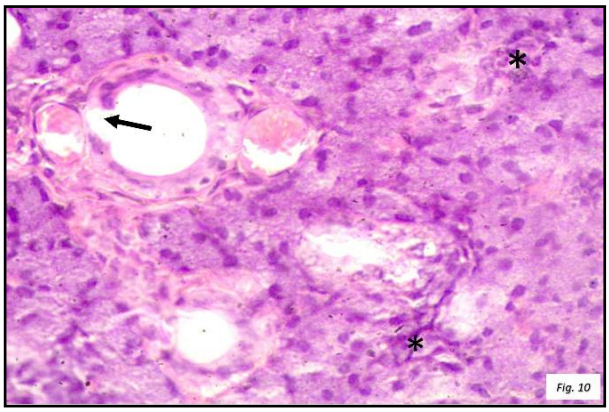

Figure 10: A photomicrograph of a section of rat's submandibular gland of group II (MTX group) showing disarrangement and indistinct outline of most of the acini together with numerous aggregations of closely packed disorganized cells (*). Notice the loss of ductal regular cellular arrangement, ill-defined nuclei and the area of focal detachment of ductal epithelial lining (↑). (H&E x 400)

Immune stained sections for Ki-67 protein revealed very weak positive reaction which was dispersed in ill-defined areas Figure (11).

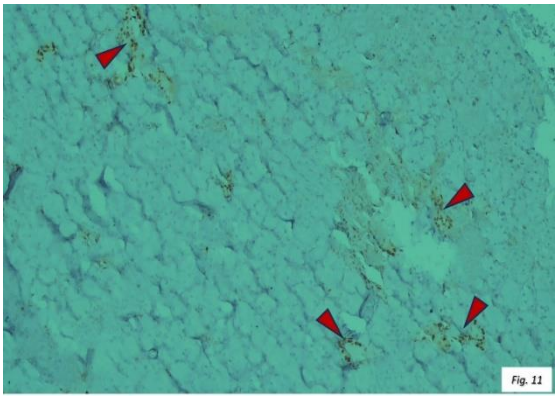

Figure 11: A photomicrograph of a section of rat's submandibular gland of group II (MTX group) showing very weak reaction to Ki-67 protein dispersed in few ill-defined areas. (Anti Ki-67 antibodies immunostaining X100)

Semithin sections showed loss of distinct cell boundaries Figures (12&13). The cytoplasm appeared rarefied Figure (13) with lack of their regular basal nuclear arrangement and most of them appeared deeply stained and irregular in shape Figures (12&13). Striated ducts revealed evident cytoplasmic vacuolation, irregular nuclei and loss of their characteristic basal striations Figure (12). Some neighboring ducts showed also marked variation in their nuclear shape and size (anisonucleosis) in addition to many cytoplasmic vacuoles Figure (12). Widespread dilated congested blood vessels were seen among glandular acini and ducts Figure (13).

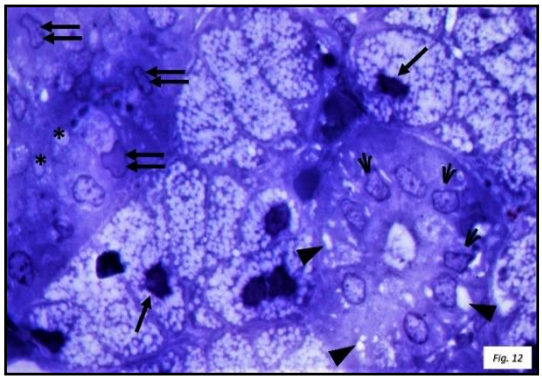

Figure 12: A photomicrograph of a section of rat's submandibular gland of group II (MTX group) showing acini with indistinct cell boundaries enclosing irregular deeply stained nuclei (↑). Notice the striated duct with irregular nuclei (⇑), cytoplasmic vacuolation (Δ) and indistinct basal striations. Note also the nearby duct with cytoplasmic vacuoles (*) and anisonucleosis (↑↑). (Toluidine blue x 1000)

Figure 13: A photomicrograph of a section of rat's submandibular gland of group II (MTX group) showing acini with indistinct cell boundaries, rarified cytoplasm and irregular nuclei of acini (↑). Notice the numerous dilated congested blood vessels (Δ) among glandular acini and ducts. (Toluidine blue x 1000)

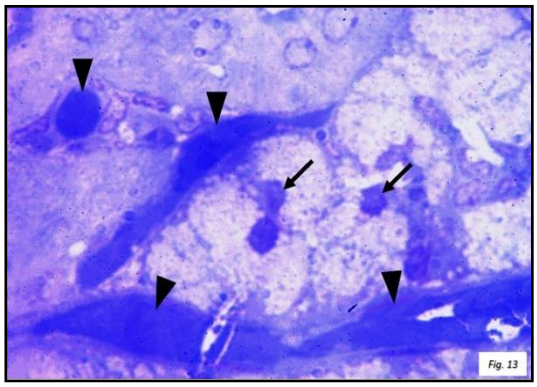

Ultrastructural examination revealed that acini had irregular thickened basal lamina Figure (14). Most of acinar cells' nuclei were irregular heterochromatic with patchy chromatin condensation Figures (14&15), other nuclei showed different degrees of degeneration ranging from karyorrhexis Figure (15) up to karyolysis Figure (16). The surrounding cytoplasm showed obvious vacuolation Figures (14,15&16), indistinct cytoplasmic organelles Figure (14) apart from markedly dilated rER Figure (16), ballooned mitochondria where many of them had distorted cristae Figure (15) and many others appeared coalesced together with indistinct Figure (15) or irregular outline Figure (16). Moreover, the large, rounded apical electron dense secretory granules appeared to be less numerous Figure (14).

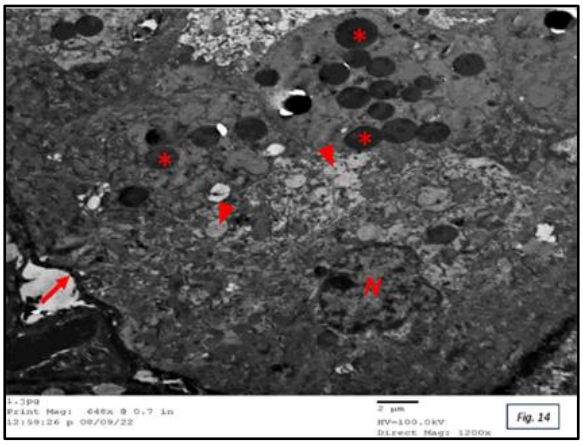

Figure 14: An electronmicrograph of a section of rat's submandibular gland of group II (MTX group) showing acinus with irregular heterochromatic nucleus (N) with patchy chromatin condensation, cytoplasmic vacuolation (Δ) and indistinct organelles. Notice the few large, rounded apical electron dense secretory granules (*). Note also the irregular thickened basal lamina (↑). (Uranyl acetate & lead citrate x1200)

Figure 15: An electronmicrograph of a section of rat's submandibular gland of group II (MTX group) showing acinar cells with irregular heterochromatic nucleus (N) with patchy chromatin condensation and an adjacent one showing karyorrhexis (n). Notice the surrounding cytoplasmic vacuolation (Δ), the ballooned mitochondria with distorted cristae (m) and the coalesced ones with indistinct outline (↑). (Uranyl acetate & lead citrate x4000)

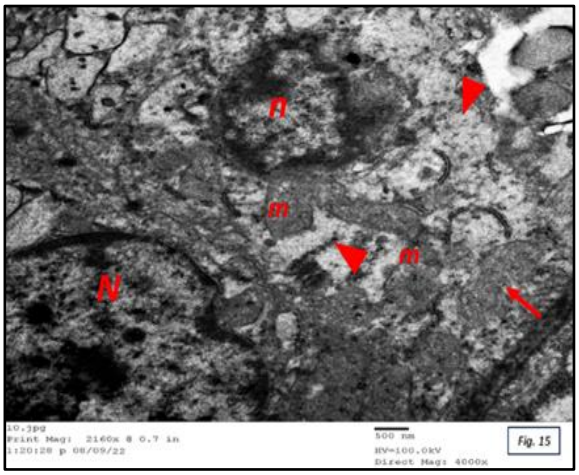

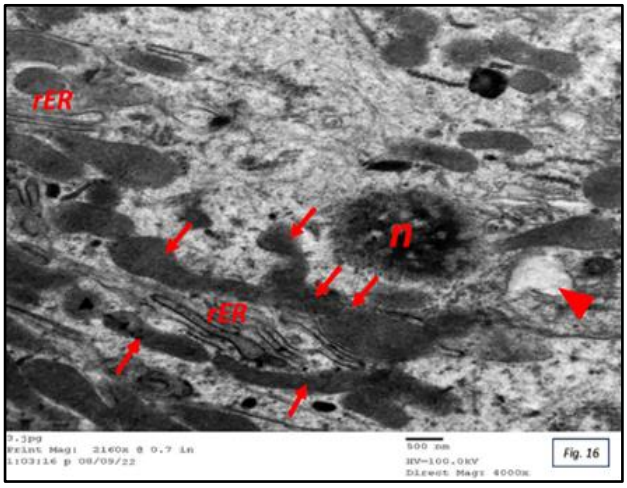

Figure 16: An electronmicrograph of a section of rat's submandibular gland of group II (MTX group) showing acinar cell with karyolitic nucleus (n) with surrounding cytoplasmic vacuoles (Δ) and dilated rER (rER). Notice the coalesced mitochondria with irregular outline (↑). (Uranyl acetate & lead citrate x4000)

Striated ducts had irregular thickened basal lamina, evident distortion of their characteristic basal infoldings and subsequent loss of the incorporated arrays of aligned mitochondria Figure (17). Adjacent mitochondria appeared ballooned with distorted cristae Figure (18). Nuclei also revealed marked variability in their positions, shapes, sizes, chromatin condensation. Some appeared almost rounded or irregular with patchy chromatin Figure (17) and others were irregular, shrunken with peripheral chromatin condensation Figures (17&18). Moreover, dilated rER Figure (18) together with wide vacuolar areas Figures (17&18) were frequently encountered. In addition, few apical vesicles with variable sizes and electron densities were observed Figure (18).

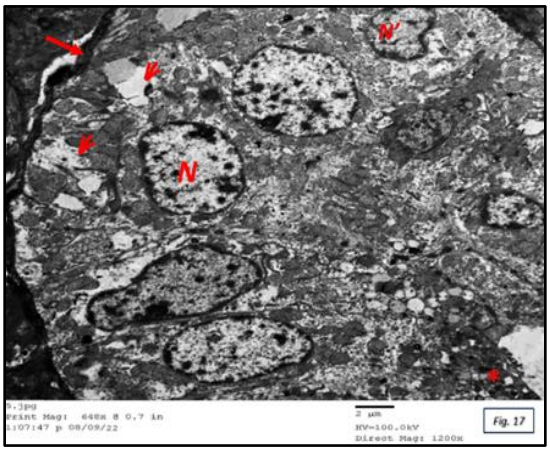

Figure 17: An electronmicrograph of a section of rat's submandibular gland of group II (MTX group) showing striated duct with thickened and irregular basal lamina (↑), loss of characteristic basal infoldings. Notice the almost rounded and irregular nuclei (N) with patchy chromatin and the shrunken irregular one (N'). Note also the few apical secretory granules (*) with variable sizes and electron densities and the wide vacuolar areas (⇑). (Uranyl acetate & lead citrate x1200)

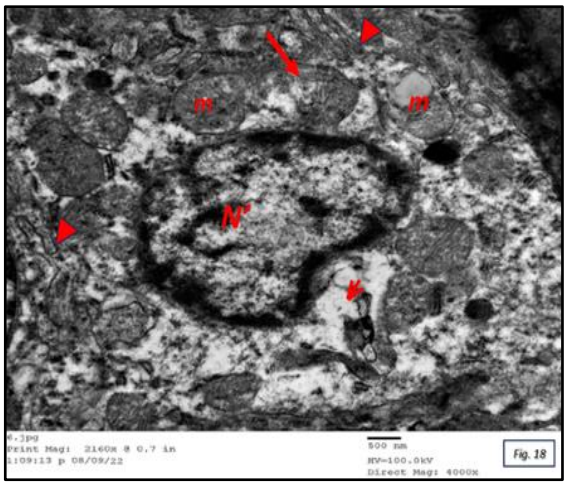

Figure 18: An Electronmicrograph of a section of rat's submandibular gland of group II (MTX group) showing shrunken irregular nucleus (N') surrounded by wide vacuolar areas (⇑), ballooned mitochondria (m) with distorted cristae (↑) and dilated rER (Δ). (Uranyl acetate & lead citrate x4000)

☆ ***Group III (MTX and LC treated Group):***

Light microscopic examination of H&E-stained sections revealed almost preserved architecture in most fields apart from some areas of separation in glandular tissue Figure (19). Some acini had well defined outline with almost rounded basal nuclei. However, others had indistinct outline and disorganized nuclear arrangement Figure (20). In addition, groups of overcrowded cells were also observed among the acini Figures (19&20). Striated ducts had almost clear outline, rounded lumen and well defined, yet disorganized, rounded to oval nuclei Figure (20). Widespread cytoplasmic vacuolation was also observed in most of them. Moreover, aggregations of connective tissue fibers studded with cellular infiltration were still encountered Figure (19).

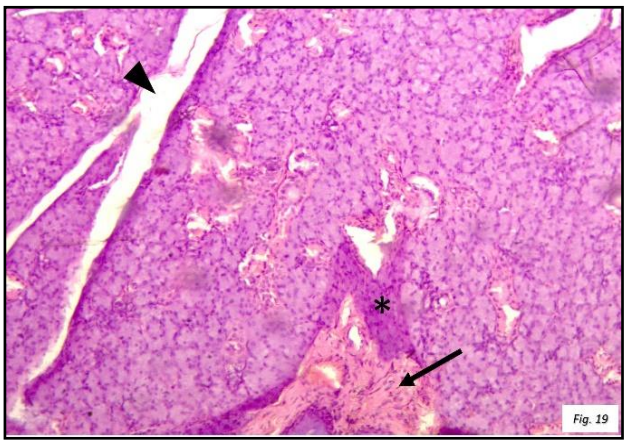

Figure 19: A photomicrograph of a section of rat's submandibular gland of group III (MTX and LC group) showing almost preserved architecture with some areas of separation in glandular tissue (Δ). Notice the groups of overcrowded cells (*) among the acini and the adjacent aggregation of connective tissue fibers (↑) studded with cellular infiltration. (H&E x 100)

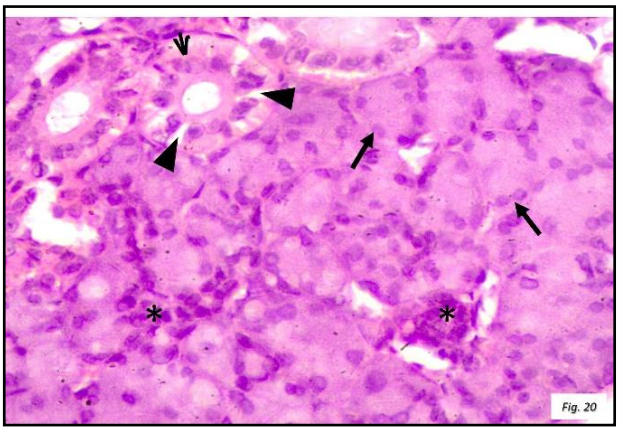

Figure 20: A photomicrograph of a section of rat's submandibular gland of group III (MTX and LC group) showing some acini with welldefined outline containing rounded basal nuclei (↑) and others with indistinct outline and disorganized nuclear arrangement. Notice the groups of overcrowded cells among the acini (*). Note also the striated ducts with almost clear outline, rounded lumen and well defined, yet disorganized, rounded to oval nuclei and widespread cytoplasmic vacuolation (Δ). (H&E X400)

Immune stained sections for Ki-67 protein showed positive reaction in some ducts in addition to few dispersed areas Figure (21).

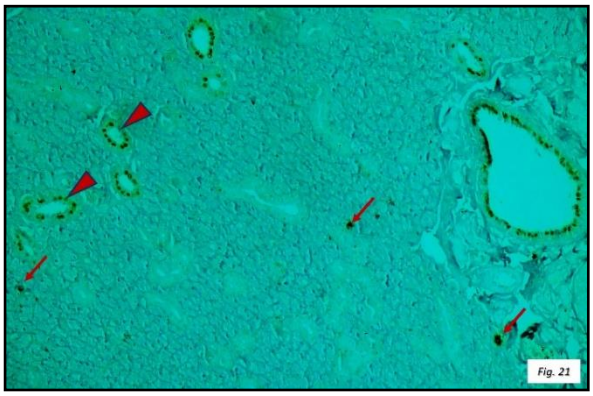

Figure 21: A photomicrograph of a section of rat's submandibular gland of group III (MTX and LC group) showing positive reaction to Ki-67 protein in some ducts in addition to few dispersed areas. (Anti Ki-67 antibodies immunostaining X100)

Semithin sections revealed almost well-defined acini lined by pyramidal cells with pale stained cytoplasm and rounded to oval nuclei, apart from some small, distorted nuclei. Striated ducts appeared lined by columnar cells with preserved basal striations and almost central rounded and vesicular nuclei Figure (22).

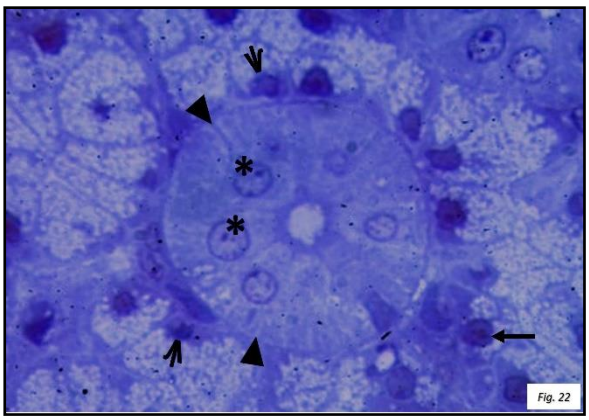

Figure 22: A photomicrograph of a section of rat's submandibular gland of group III (MTX and LC group) showing acini with rounded to oval nuclei (↑) and small, distorted ones (⇑). Notice the striated ducts lined by columnar cells with basal striations (Δ) and almost central rounded and vesicular nuclei (*). (Toluidine blue x 1000)

Ultrastructural examination showed that the acini had rounded to oval euchromatic nuclei with prominent nucleoli and perinuclear rounded to oval mitochondria. Numerous large almost prominent rounded electron dense secretory granules were seen at the apical parts of the acinar cells. The luminal surface had apical projecting microvilli. Myoepithelial cells with flattened heterochromatic nuclei were observed at the basal aspect of the acini. However, nearby dilated congested blood vessels were still seen Figure (23).

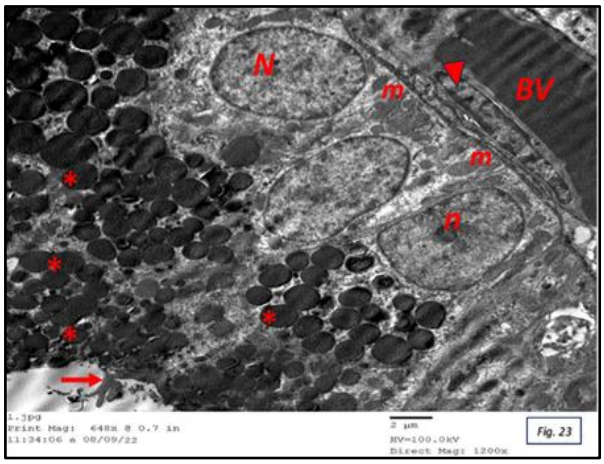

Figure 23: An electronmicrograph of a section of rat's submandibular gland of group III (MTX and LC group) showing acinar cells with rounded to oval euchromatic nuclei (N) with prominent nucleoli (n) in one of them with paranuclear rounded to oval mitochondria (m). Notice the numerous large almost rounded electron dense secretory granules (*) at the apical parts of the acinar cells and the projecting microvilli (↑). Note also the myoepithelial cell with flattened heterochromatic nucleus (Δ) and the nearby dilated congested blood vessel (BV). (Uranyl acetate & lead citrate x1200)

Striated ductal cells had almost rounded euochromatic nuclei Figures (24&25) with adjacent closely packed arrays or rER and numerous rounded to oval mitochondria Figure (25). Some of these perinuclear mitochondria appeared touching or even encroaching on the nuclear membrane Figure (24). The basal side of cells revealed that the ducts had thick regular and well-defined basal lamina with partial preservation of the basal infoldings interdigitating with few regular rounded to oval mitochondria. However, ballooned mitochondria with ruptured cristae and some coalesced ones with markedly irregular outline were also seen Figure (25). The apical side appeared with some irregular mitochondria Figure (25) and ad luminal small, rounded vesicles with variable sizes and electron densities together with apical finger like projecting microvilli Figure (24).

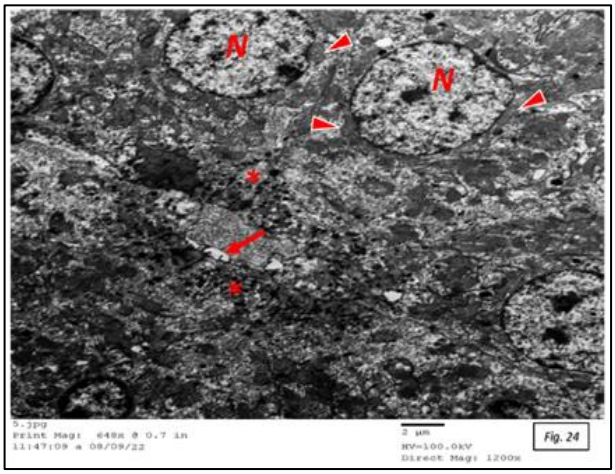

Figure 24: An electronmicrograph of a section of rat's submandibular gland of group III (MTX and LC group) showing striated duct with almost rounded euochromatic nuclei (N), small apical secretory granules (*) with variable sizes and electron densities and finger like projecting microvilli (↑). (Uranyl acetate & lead citrate x1200)

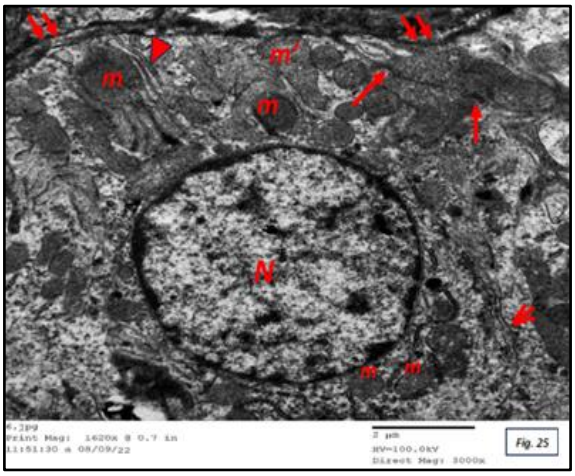

Figure 25: An electronmicrograph of a section of rat's submandibular gland of group III (MTX and LC group) showing striated duct with almost rounded euochromatic nucleus (N) with adjacent rounded to oval mitochondria (m) and closely packed arrays of rER (⇑). Notice the thick regular basal lamina (↑↑), basal infoldings (Δ) interdigitating with some regular rounded to oval mitochondria (m) and other ballooned ones with distorted cristae (m'). Note also the coalesced mitochondria with irregular outline (↑). (Uranyl acetate & lead citrate x3000)

➢ **Morphometric Results:**

Statistical analysis revealed no significant differences among the control subgroups.

The mean area percentage of Ki-67 immune reactivity of group II revealed a highly significant decrease when compared with those of group I. However, the mean area percentage in group III revealed a highly significant increase when compared to those of group II and a significant decrease when compared to that of group I (Table and Histogram).

Table: Showing mean area percentage of Ki-67 immune reactivity done by (student "t" test)

		Group I (Control Group)	Group II (MTX Group)	Group III (MTX and LC treated Group)
Mean area percentage (%)		7.385 ± 0.49	4.08 ±0.87	6.06 ±0.98
T test	Between Group I&II	P= 0.0000105 (P < 0.001**)		
	Between Group II&III	P= 0.0041 (P < 0.05*)		
	Between Group I&III	P= 0.015 (P < 0.05*)		

Values are expressed as Mean ± SD.
(**= Highly Significant and * = Significant)

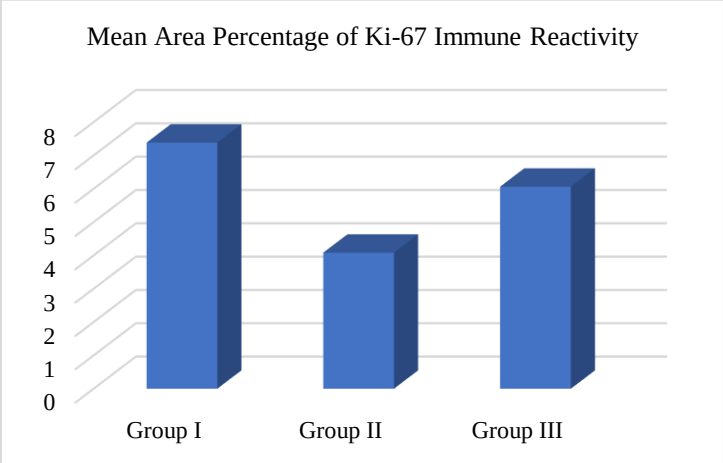

Histogram: demonstrating the morphometric comparison between the three groups as regards mean area percentage of Ki-67 immune reactivity.

DISCUSSION:

Submandibular gland hypofunction is considered one of the side effects of MTX; a golden member in chemotherapeutic agents and a chief drug in the treatment of RA, which already manifests by dry mouth. The marked decline in submandibular function with subsequent affection of the general well-being of cancer as well as RA patients receiving MTX [(4)] made it mandatory to investigate the mechanism of MTX induced submandibular hypofunction and search for different agents to protect the gland against these hazardous effects.

The present study manifested the marked destructive effects of MTX on submandibular gland including evident loss of glandular architectures and marked separation of glandular tissue together with evident structural alterations in both the acinar and the ductal sides. Acinar cells showed marked cytoplasmic vacuolation with indistinct cytoplasmic organelles, ballooned mitochondria together with degenerative nuclear changes ranging from

irregular nuclei with heterochromatic chromatin condensation up to karyorrhexis and karyolysis. Striated ducts also revealed thickened and irregular lining, together with wide vacuolar areas, ballooned mitochondria with distorted cristae, dilated rER, in addition to the presence of shrunken nuclei.

Being a folic acid antagonist, MTX acts by reducing the activity of many folate-dependent enzymes, with subsequent inhibition of DNA synthesis, repair, and cellular proliferation [(21)].

Moreover, it has been found to cause a marked decline in the level of antioxidant enzymes including glutathione peroxidase, superoxide dismutase, and catalase. This results in a decrease in the level of the reduced form of Glutathione and elevation of oxidative stress markers as malondialdehyde and Nitric oxide free radicals [(22)]. This oxidant/antioxidant imbalance leads to the release of free radicals during its intracellular metabolism. This has been found to exert a negative impact on the cellular integrity resulting in lipid peroxidation leading to lysis of cell organelles and plasma membranes with subsequent release of these free radicals into the serum [(23&24)]. This could explain the indistinct cytoplasmic organelles, dilated rER, ruptured mitochondrial cristae and the vacuolar spaces noted in the present study.

This MTX induced cellular damage was further emphasized in this study by the highly significant decrease in Ki-67 immune reactivity of group II compared to the control group. Ki-67 is a nuclear nonhistone protein present in all active phases of cell cycle, except the G0 phase and its presence is considered as a sign of proliferation [(25&26)]. It has been reported that Ki-67 immuno-expression was positive within the acini and ducts of the submandibular gland [(27)]. However, *Mansy et al., 2020* observed that the Ki-67 positive immuno-expression was more distinctive in the duct system rather than the acinar one [(28)]. This was similar to the findings of the present study where the control group showed that the positive reaction was more evident in the glandular ductal system with scattered nuclear reactivities in few secretory acini. On the other hand, the present study revealed very weak positive reaction which was dispersed in ill-defined areas. Chemotherapeutic drugs have been found to cause evident reduction in Ki-67 proliferation index reflecting their anti-proliferative impacts on tumor cells [(29)]. It has been reported that MTX induced marked decrease in Ki-67 immune reaction in hippocampal regions reflecting its strong anti-proliferative effects [(30)]. This could further emphasize the degenerative nuclear changes encountered in the MTX group in the current study including irregular nuclei with heterochromatin condensation, karyorrhexis and eventually karyolysis with associated degenerative cytoplasmic changes.

Cytoplasmic vacuolation has been considered as one of the primary responses to all forms of cell injury [(31)]. However, MTX associated widespread cytoplasmic vacuolation that were evident in both acinar and ductal cells has been also attributed to the swollen mitochondria with damaged cristae [(32&33)].

Ballooned and distorted mitochondria with distorted cristae were also frequently seen at the basal side of striated ducts in this group with loss of their incorporation between the basal infoldings leading to disappearance of the characteristic basal striations of these ducts. Moreover, their apical rounded vesicles appeared to be less numerous with variables sizes and electron densities. Similar findings were reported in the striated ducts of parotid gland following MTX administration [(6)]. These findings could be attributed to MTX-induced degeneration of these cells as a consequence of free radicals and ROS generation [(34)].

Additionally, it has been stated that the salivary components produced by the acinar cells were incorporated into the striated ducts

and their cells which are specialized in the secretion and resorption of electrolytes and their transport in a bidirectional manner between the ductal lumen and the extracellular spaces. Moreover, their apical vesicles have been proved to be involved in transcytosis of secretory immunoglobulin (IgA) from the basolateral to apical lumen thus, they are considered to be the histochemical markers for the efficient endocytosis and transcytosis processes [(35)]. Being rich in many immunoglobins, especially IgA, saliva plays an important role in the immunologic defence mechanism of oropharynx against microorganisms [(36)]. Thus, any change in the density of these apical vesicles and the characteristic basal infolding as noted in the present study could denote disturbance in striated ductal function and explain the MTX associated disturbance in the oral hygiene and increased susceptibility to infection.

The present study also revealed marked decrease in the acinar secretory granules with thinning and decreased density of their apical microvilli. These findings could reflect the MTX induced hyposecretory state. It has been established that MTX binds to dihydrofolic reductase thus preventing the conversion of folic to its active folinic acid form. This, in turn, hinders nucleic acids, amino acids and proteins synthesis with consequent membrane damage, cellular death and altered salivary secretion [(6)].

In addition, this group also showed aggregation of connective tissue fibers studded with cellular infiltrates. This could be also attributed to the MTX induced inflammatory state evidenced by its associated elevation of serum levels of proinflammatory cytokines including Tumor necrosis factor alpha, interleukin 1 beta, and interleukin 6 [(22)]. It has been also reported that these inflammatory cytokines lead to cellular differentiation into myofibroblasts, with extracellular matrix components deposition which was proposed as the explanation of the pronounced fibrosis observed following MTX administration [(37)].

Moreover, vascular congestion was an almost constant finding in this group's different section. It has been previously reported that granular degradation, inflammatory cell infiltration, and vascular congestion were among the hazards following MTX administration [(38)]. It has been also postulated that the goal of these inflammatory responses was to increase blood flow to the damaged areas of the body [(39)]. This dilatation and congestion could be also attributed to the MTX associated inflammatory reaction which leads to an increase in the trans endothelial permeability [(6)].

On the other hand, examination of group III (MTX and LC treated Group) revealed marked preservation of the glandular architecture and ultrastructure. Most of the acini and striated ducts had almost preserved outline with rounded to oval nuclei and well defined lumina apart from others with indistinct outline. Acini showed numerous secretory granules with apical microvilli. Striated ducts had almost preserved basal striations, but with some intervening ballooned mitochondria and others with distorted cristae with apical small, rounded vesicles with variable sizes and electron densities together with apical finger like projecting microvilli. However, groups of overcrowded cells and aggregations of connective tissue fibers studded with cellular infiltration were still observed among the acini. Moreover, this group specifically showed mitochondria in close proximity and even encroaching on the nuclear membrane. *Prachar, (2003)* previously reported that physical mitochondrial-nuclear contact could act as an energy reservoir for mRNA and protein transport which denotes cellular metabolic activity [(40)]. It has ben also postulated that this proximity is an energy communication contact required due to the high-energy demands of the nucleus [(41)]. This

could reflect LC associated cellular attempts to overcome MTX-induced toxicity.

These LC protective effects were further emphasized by the significant increase in Ki- 67 immune reactivity of group III compared to the MTX group. However, this increase in immune reactivity was still not back to the normal level where there was a persistent significant decrease in the immune staining of group III when compared to the control group.

These findings revealed the potent protective role of LC against MTX toxicity on submandibular gland structure and subsequently its function. This protective role could be attributed to the fact that LC acts as an essential cofactor aiding in the transport of free fatty acids to the mitochondria where beta-oxidation occurs leading to the production of acetyl- CoA which is a crucial precursor for the Krebs cycle [(42)]. This helps in the production of ATP which plays a pivotal role in oxidative system balance, antiperoxidative activity, and superoxide anion formation inhibition [(7)].

In addition, it has been stated that LC has anti-inflammatory [(43)] and antiapoptotic effects [(44)]. It has been also recently proved to reduce the oxidative and apoptotic markers in peripheral organs of rats [(45&46)]. These facts could explain the ameliorative effects exerted by LC in the present study both on the glandular architecture as well as the acinar and ductal ultrastructure.

Conclusion:

Methotrexate led to marked histoarchitectural and ultrastructural changes in submandibular gland. However, MTX administration under the umbrella of LC markedly decreased such changes. Thus, LC could be considered as a highly promising protective agent against MTX-induced xerostomia in cancer and RA arthritis patients.

Conflict of Interest:

No conflict of interest.

REFERENCES:

1. **Chaveli-López B.** Oral toxicity produced by chemotherapy: A systematic review. J Clin Exp Dent. 2014 Feb 1;6(1):e81-90. doi: 10.4317/jced.51337. PMID: 24596641; PMCID: PMC3935911.
2. **Hamed KM, Dighriri IM, Baomar AF, Alharthy BT, Alenazi FE, Alali GH, Alenazy RH, Alhumaidi NT, Alhulayfi DH, Alotaibi YB, Alhumaidan SS, Alhaddad ZA, Humadi AA, Alzahrani SA, Alobaid RH.** Overview of Methotrexate Toxicity: A Comprehensive Literature Review. Cureus. 2022 Sep 23;14(9):e29518. doi: 10.7759/cureus.29518. PMID: 36312688; PMCID: PMC9595261.
3. **Koźmiński P, Halik PK, Chesori R, Gniazdowska E.** Overview of dual-acting drug methotrexate in different neurological diseases, autoimmune pathologies and cancers. International Journal of Molecular Sciences. 2020;21(10) doi: 10.3390/ijms21103483.3483
4. **Ungureanu LB, Grădinaru I, Ghiciuc CM, Amălinei C, Geleţu GL, Petrovici CG, Stănescu RŞ.** Atrophy and Inflammatory Changes in Salivary Glands Induced by Oxidative Stress after Exposure to Drugs and Other Chemical Substances: A Systematic Review. Medicina (Kaunas). 2023 Sep 21;59(9):1692. doi: 10.3390/medicina59091692. PMID: 37763811; PMCID: PMC10535338.
5. **Ottaviani G, Targato G, Rupel K, Gobbo M, Generali D, Guglielmi A, Dicorato A, Adamo D, Canfora F, Di Lenarda R, Biasotto M.** Oral Problems in Oncology Patients Undergoing Chemotherapy for Solid Tumors: A Prospective Observational Study. Cancers (Basel). 2023 Dec 29;16(1):176. doi: 10.3390/cancers16010176. PMID: 38201603; PMCID: PMC10778343.
6. **Omar AI, Yousry MM, and EA Farag.** Therapeutic mechanisms of granulocyte-colony stimulating factor in methotrexate-

induced parotid lesion in adult rats and possible role of telocytes: a histological study. Egyptian Journal of Histology. 2018; vol. 41, no. 1, pp. 93–107.

7. **Sener G, Ekşioğlu-Demiralp E, Cetiner M, Ercan F, Sirvanci S, Gedik N, Yeğen BC.** L-Carnitine ameliorates methotrexate-induced oxidative organ injury and inhibits leukocyte death. Cell Biol Toxicol. 2006 Jan;22(1):47-60. doi: 10.1007/s10565-006-0025-0. PMID: 16463019
8. **Reuter SE, Evans AM. Carnitine and acylcarnitines.** pharmacokinetic, pharmacological and clinical aspects. Clin Pharmacokinet. 2012 Sep 1;51(9):553-572. doi: 10.1007/BF03261931. PMID: 22804748.
9. **Cave MC, Hurt RT, Frazier TH, Matheson PJ, Garrison RN, McClain CJ, McClave SA.** Obesity, inflammation, and the potential application of pharmaconutrition. Nutr Clin Pract. 2008 Feb;23(1):16-34. doi: 10.1177/011542650802300116. PMID: 18203961.
10. **Alhasaniah AH.** l-carnitine: Nutrition, pathology, and health benefits. Saudi J Biol Sci. 2023 Feb;30(2):103555. doi: 10.1016/j.sjbs.2022.103555. Epub 2022 Dec 30. PMID: 36632072; PMCID: PMC9827390.
11. **Bonomini M, Zammit V, Pusey CD, De Vecchi A, Arduini A.** Pharmacological use of L-carnitine in uremic anemia: has its full potential been exploited? Pharmacol Res. 2011 Mar;63(3):157-164. doi: 10.1016/j.phrs.2010.11.006. Epub 2010 Dec 4. PMID: 21138768.
12. **Gao X, Sun G, Randell E, Tian Y, Zhou H.** Systematic investigation of the relationships of trimethylamine N-oxide and L-carnitine with obesity in both humans and rodents. Food Funct. 2020 Sep 23;11(9):7707-7716. doi: 10.1039/d0fo01743d. PMID: 32915186.
13. **Van Weyenberg S, Buyse J, Janssens GP.** Increased plasma leptin through l-carnitine supplementation is associated with an enhanced glucose tolerance in healthy ponies. J Anim Physiol Anim Nutr (Berl). 2009 Apr;93(2):203-208. doi: 10.1111/j.1439-0396.2008.00807. x. PMID: 19320933.
14. **Koppula S, Kumar H, More SV, Kim BW, Kim IS, Choi DK.** Recent advances on the neuroprotective potential of antioxidants in experimental models of Parkinson's disease. Int J Mol Sci. 2012;13(8):10608-10629. doi: 10.3390/ijms130810608. Epub 2012 Aug 23. PMID: 22949883; PMCID: PMC3431881.
15. **Sayed-Ahmed M.M.**, Role of carnitine in cancer chemotherapy-induced multiple organ toxicity. Saudi Pharm. J. 18 (2010) 195–206, https://doi.org/10.1016/j. jsps.2010.07.008.
16. **Katturajan R, Evan Prince S.** L-carnitine and Zinc supplementation impedes intestinal damage in MTX-treated adjuvant-induced arthritis rats: Reinstating enterocyte proliferation and trace elements. J Trace Elem Med Biol. 2023 Jul; 78:127188. doi: 10.1016/j.jtemb.2023.127188. Epub 2023 Apr 28. PMID: 37163819.
17. **Bodea F, Bocea A, Decea N.** L-carnitine decreases oxidative stress induced by experimental hypobaric hypoxia. Pediatr Endocrinol Diabetes Metab. 2010;16(2):78-81. PMID: 20813083.
18. **Bancroft JD and Layton C**. The Hematoxylin and eosin. In: Suvarna SK, Layton C and Bancroft JD editors. Theory and Practice of histological techniques. 7th ed., Churchill Livingstone of El Sevier. Philadelphia. Ch. (2013) pp: 172 - 426.
19. **Abdel-Kareem RH, Hulail ME, El-Sherbiny EMK, and Abdelwahab OA**. Dose-Duration Dependent Changes Induced by Atrazine in the Ovary of Adult Albino Rat and the Possible Protective Role of L-Carnitine: Histological and Immunohistochemical Study. Egyptian journal of Histology;Volume 46, Issue 1, March 2023, Page 414-443. DOI: 10.21608/ejh.2021.92935.1551
20. **Suvarna SK, Layton C and Bancroft JD.** Bancroft's theory and practice of histological techniques. 7th ed. Churchill Livingstone. ElSevier. 2013; 224, 408-411.
21. **Jensen SB, Pedersen AM, Reibel J, Nauntofte B.** Xerostomia and hypofunction of the salivary glands in cancer therapy.

Support Care Cancer. 2003 Apr;11(4):207-225. doi: 10.1007/s00520-002-0407-7. Epub 2002 Nov 23. PMID: 12673459.

22. **Drishya S, Dhanisha SS, Guruvayoorappan C.** Antioxidant-rich fraction of Amomum subulatum fruits mitigates experimental methotrexate-induced oxidative stress by regulating TNF-α, IL-1β, and IL-6 proinflammatory cytokines. J Food Biochem. 2022 Apr;46(4):e13855. doi: 10.1111/jfbc.13855. Epub 2021 Jul 11. PMID: 34250612.
23. **EL-Agamy AA, Afifi OK and Sheta AA.** Protective role of panax gensing on fluvoxamine maleate induced structural changes in the submandibular salivary gland of rats. Nature and Science, 2014 vol. 12, no. 4: 21–29.
24. **Sajith M, Pawar A, Bafna V, Bartakke S, Subramanian K, Vaidya N.** Serum Methotrexate Level and Side Effects of High Dose Methotrexate Infusion in Pediatric Patients with Acute Lymphoblastic Leukaemia (ALL). Indian J Hematol Blood Transfus. 2020 Jan;36(1):51-58. doi: 10.1007/s12288-019-01144-3. Epub 2019 Jun 6. PMID: 32174691; PMCID: PMC7042471.
25. **Nishimura R, Osako T, Okumura Y, Hayashi M, Toyozumi Y, Arima N.** Ki-67 as a prognostic marker according to breast cancer subtype and a predictor of recurrence time in primary breast cancer. Exp Ther Med. 2010 Sep;1(5):747-754. doi: 10.3892/etm.2010.133. Epub 2010 Jul 21. PMID: 22993598; PMCID: PMC3445951.
26. **Faur AC, Sas I, Motoc AG, Cornianu M, Zamfir CL, Lazăr DC, Folescu R.** Ki-67 and p53 immunostaining assessment of proliferative activity in salivary tumors. Rom J Morphol Embryol. 2015;56(4):1429-39. PMID: 26743291.
27. **Dayan D, Vered M, Sivor S, Hiss Y, Buchner A.** Age-related changes in proliferative markers in labial salivary glands: a study of argyrophilic nucleolar organizer regions (AgNORs) and Ki-67. Exp Gerontol. 2002 Jun;37(6):841-850. doi: 10.1016/s0531-5565(02)00019-0. PMID: 12175484.
28. **Mansy M, Soliman M, Mubarak R, Shamel M.** The role of exogenous epidermal growth factor on Ki-67 proliferation marker expression in the submandibular salivary gland of albino rats receiving doxorubicin. F1000Res. 2020 Dec 3; 9:1393. doi: 10.12688/f1000research.27186.1. PMID: 33456767; PMCID: PMC7797936.
29. **Miller WR, White S, Dixon JM, Murray J, Renshaw L, Anderson TJ.** Proliferation, steroid receptors and clinical/pathological response in breast cancer treated with letrozole. Br J Cancer. 2006 Apr 10;94(7):1051-6. doi: 10.1038/sj.bjc.6603001. PMID: 16538221; PMCID: PMC2361236.
30. **Sritawan N, Prajit R, Chaisawang P, Sirichoat A, Pannangrong W, Wigmore P, Welbat JU.** Metformin alleviates memory and hippocampal neurogenesis decline induced by methotrexate chemotherapy in a rat model. Biomed Pharmacother. 2020 Nov; 131:110651. doi: 10.1016/j.biopha.2020.110651. Epub 2020 Aug 22. PMID: 32841896.
31. **Suriyakumari KVP, Udayakumar R and Ruba T:** Histological investigations on kidney of sildenafil citrate (edegra) treated albino mice. Int. J. Anat. Res. (2016) 4 (1): 1977-1980.
32. **Mohsen R.O.M. and El-Messiry H.** The Possible Ameliorating Role of Platelet Rich Plasma versus Propolis on Submandibular Salivary Glands Damage Induced by Methotrexate in Adult Male Albino rats (Light and Transmission Electron Microscopic Study). EJH- Volume 46, Issue 2, June 2023, Page 993-1006.
33. **Lombaert IM, Brunsting JF, Wierenga PK, Kampinga HH, de Haan G, Coppes RP.** Cytokine treatment improves parenchymal and vascular damage of salivary glands after irradiation. Clin Cancer Res. 2008 Dec 1;14(23):7741-7750. doi: 10.1158/1078-0432.CCR-08-1449. PMID: 19047101.
34. **Solenski NJ, diPierro CG, Trimmer PA, Kwan AL, Helm GA.** Ultrastructural changes of neuronal mitochondria after transient and permanent cerebral ischemia.

Stroke. 2002 Mar;33(3):816-24. doi: 10.1161/hs0302.104541. Erratum in: Stroke 2002 Apr;33(4):1171. Helms Gregory A [corrected to Helm Gregory A]. PMID: 11872909.

35. **Tandler B, Gresik EW, Nagato T, Phillips CJ.** Secretion by striated ducts of mammalian major salivary glands: review from an ultrastructural, functional, and evolutionary perspective. Anat Rec. 2001 Oct 1;264(2):121-145. doi: 10.1002/ar.1108. PMID: 11590591.
36. **Iorgulescu G.** Saliva between normal and pathological. Important factors in determining systemic and oral health. J Med Life. 2009 Jul-Sep;2(3):303-307. PMID: 20112475; PMCID: PMC5052503**.**
37. **Braicu C, Ladomery MR, Chedea VS, Irimie A, Berindan-Neagoe I.** The relationship between the structure and biological actions of green tea catechins. Food Chem. 2013 Dec 1;141(3):3282-3289. doi: 10.1016/j.foodchem.2013.05.122. Epub 2013 Jun 4. PMID: 23871088.
38. **Hsu PC, Hour TC, Liao YF, Hung YC, Liu CC, Chang WH, Kao MC, Tsay GJ, Hung HC, Liu GY.** Increasing ornithine decarboxylase activity is another way of prolactin preventing methotrexate-induced apoptosis: crosstalk between ODC and BCL-2. Apoptosis. 2006 Mar;11(3):389-399. doi: 10.1007/s10495-006-4002-0. PMID: 16520895.
39. **Taha RM, Abdel-Latif GA, Said RH.** The Prospective Effect of Green Tea versus Pomegranate Peels Extracts on Submandibular Salivary Glands of Albino Rats after Methotrexate Administration (Histological and Immunohistochemical Study). Int J Dent. 2024 Jan 3; 2024:3290187. doi: 10.1155/2024/3290187. PMID: 38213552; PMCID: PMC10781530.
40. **Prachar J.** Intimate contacts of mitochondria with nuclear envelope as a potential energy gateway for nucleo-cytoplasmic mRNA transport. Gen Physiol Biophys. 2003 Dec;22(4):525-34. PMID: 15113124.
41. **Dzeja PP, Bortolon R, Perez-Terzic C, Holmuhamedov EL, Terzic A.** Energetic communication between mitochondria and nucleus directed by catalyzed phosphotransfer. Proc Natl Acad Sci U S A. 2002 Jul 23;99(15):10156-10161. doi: 10.1073/pnas.152259999. Epub 2002 Jul 15. PMID: 12119406; PMCID: PMC126640.
42. **Longo N, Frigeni M, Pasquali M.** Carnitine transport and fatty acid oxidation. Biochim Biophys Acta. 2016 Oct;1863(10):2422-2435. doi: 10.1016/j.bbamcr.2016.01.023. Epub 2016 Jan 29. PMID: 26828774; PMCID: PMC4967041.
43. **Zanelli SA, Solenski NJ, Rosenthal RE, Fiskum G.** Mechanisms of ischemic neuroprotection by acetyl-L-carnitine. Ann N Y Acad Sci. 2005 Aug; 1053:153-161. doi: 10.1196/annals.1344.013. PMID: 16179519; PMCID: PMC4454400.
44. **Ishii T, Shimpo Y, Matsuoka Y, Kinoshita K.** Anti-apoptotic effect of acetyl-l-carnitine and l-carnitine in primary cultured neurons. Jpn J Pharmacol. 2000 Jun;83(2):119-124. doi: 10.1254/jjp.83.119. PMID: 10928324.
45. **Kelek SE, Afşar E, Akçay G, Danışman B, Aslan M.** Effect of chronic L-carnitine supplementation on carnitine levels, oxidative stress and apoptotic markers in peripheral organs of adult Wistar rats. Food Chem Toxicol. 2019 Dec; 134:110851. doi: 10.1016/j.fct.2019.110851. Epub 2019 Sep 27. PMID: 31568849.
46. **Er H, Gemici A, Tas GG, Sati L, Zengin G, Bilmen S, Derin N, Kelek SE.** Acetyl-L-carnitine attenuates chronic ethanol-induced oxidative stress, ER stress and apoptosis in rat gastric tissue. Alcohol. 2023 Nov; 112:51-59. doi: 10.1016/j.alcohol.2023.07.003. Epub 2023 Jul 25. PMID: 37499932.

الدور الوقائي لـ ل-الكارنتين ضد الآثار الجانبية التي يسببها الميثوتريكسات على الغدة اللعابية تحت الفكية في ذكور الجرذان البيضاء البالغة

ماري رفعت إسحق[1] ، جمال طه عبد الهادي[1] ، إيناس هريدي أحمد[1&2]

قسم التشريح والأجنة - كلية الطب - جامعة عين شمس [1]
قسم التشريح – كليه الطب - جامعة حائل - المملكة العربية السعودية [2]

المقدمة: يعتبر الخلل الذي يحدث للغدة اللعابية تحت الفكية و ما يلحق به من جفاف الفم هو أحد الآثار الجانبية الشائعة للميثوتريكسيت في مرضى التهاب المفاصل الروماتويدي ومرضى السرطان. و يعد ل-الكارنتين هو أحد مضادات الأكسدة التي تستخدم على نطاق واسع في الوقت الحاضر للحماية من العديد من مخاطر أدوية العلاج الكيميائي.

الهدف من البحث: دراسة التأثير الوقائي المحتمل لـ ل-الكارنتين على الغدة اللعابية تحت الفكية من الآثار السلبية الناجمة عن الميثوتريكسيت.

المواد والطرق المستخدمة: تم استخدام ستة وثلاثون من ذكور الجرذان البيضاء البالغة ، التى تتراوح أعمارعهم من ٤ إلى ٦ أشهر و أوزانهم من ٢٠٠ إلى ٢٥٠ جم. و قد تم تقسيم الحيوانات إلى أربع مجموعات كالآتى:

- **المجموعة الأولى:** ضمت ٢٤ جرذاً وتم تقسيمهم بالتساوي إلى أربع مجموعات فرعية:
  - **المجموعة الفرعية أ:** تركت الجرذان دون أي تدخل.
  - **المجموعة الفرعية ب:** تلقت الجرذان حقنة واحدة من محلول ملحي داخل الصفاق.
  - **المجموعة الفرعية ج:** تلقت الجرذان الماء المقطر ، الذى استخدم فى إذابة ل-الكارنتين، عن طريق الفم مرة واحدة يوميًا لمدة 5 أيام.
  - **المجموعة الفرعية د:** تلقت الجرذان ١٠٠ ملجم/ كجم من ل-الكارنتين مرة واحدة يوميًا لمدة 5 أيام عن طريق أنبوب المعدة .
- **المجموعة الثانية:** اشتملت على ٦ جرذان تم حقنهم ٢٠ ملجم/كجم من الميثوتريكسيت داخل الصفاق في اليوم الأول من التجربة.
- **المجموعة الثالثة:** اشتملت على ٦ جرذان تم حقنهم ٢٠ ملجم/كجم من الميثوتريكسيت داخل الصفاق في اليوم الأول من التجربة كما تم اعطائهم ١٠٠ ملجم/كجم من ل-الكارنتين مرة واحدة يوميًا لمدة ٥ أيام عن طريق أنبوب المعدة.

بعد خمسة أيام، تم تخدير الحيوانات و استخراج الغدة اللعابية تحت الفكية و معالجتها لإجراء الدراسات النسيجية و الكيميائية المناعية ل Ki-67 بالإضافة إلى دراسة البنية التحتية و التحليل المورفومترى.

النتائج: كشفت الدراسة الحالية أنا الميثوتريكسيت قد أحدث تشوهًا ملحوظًا وانفصالًا في البنية النسيجية للغدة بالإضافة إلى احتقان وتجمع ألياف النسيج الضام المحملة بالخلايا. اما من ناحية البنية التحتية، فقد كشفت ان خلايا الحويصلات و القنوات المخططة اظهرت تغيرات نووية تنكسية، وفراغات واضحة في السيتوبلازم وعضيات غير واضحة. كما كشف التحليل المورفومتري عن انخفاض كبير للغاية في التعبير المناعي ل Ki-67. أما الجرذان التي أعطيت ل-الكارنتين مع الميثوتريكسيت فقد أظهرت حفاظاً على البنية النسيجية للغدة مع زيادة نسبية كبيرة في التعبير المناعي ل Ki-67.

الاستنتاج: لقد أدى ال ل-كارنيتين دورًا وقائيًا ملحوظاً ضد التغيرات الهيكلية للغدة اللعابية تحت الفكية التي يسببها الميثوتريكسيت وبالتالي، يمكن اعتباره عاملاً وقائياً واعداً للغاية ضد جفاف الفم الناجم عن الميثوتريكسيت في مرضى السرطان والتهاب المفاصل الروماتويدي.